ICAS-88-4.6.1

ACCURACY VERSUS CONVERGENCE RATES FOR A THREE DIMENSIONAL MULTISTAGE EULER CODE

Eli Turkel
School of Mathematical Sciences
Sackler Faculty of Exact Sciences
Tel-Aviv University
and
ICASE
NASA Langley Research Center
Hampton, Virginia

I. Introduction

We analyze a finite volume cell-centered scheme to solve the three dimensional Euler equations. For a uniform Cartesian mesh the scheme reduces to a standard central difference scheme. Hence, one needs to add an artificial viscosity to prevent even-odd oscillations and also to suppress oscillations in the neighborhood of steep gradients. In order to accelerate the convergence to a steady state several acceleration techniques are used. These include, local time steps, residual smoothing and a multigrid strategy. We also describe other changes to the original code that either increase the accuracy of the steady solution or else improve the convergence rate of the iteration process.

In order for the multigrid scheme to work it is essential that the errors be smoothed by the relaxation technique. Since, a central difference scheme does not include any dissipation one needs to add an artificial viscosity to damp the high modes. Hence, the artificial viscosity is needed both to give the correct shock structure in the steady state and also to eliminate high modes so that one can pass to a coarser mesh. As one increases the level of the artificial viscosity (up to some maximum) the high modes are more dissipated and the scheme converges more rapidly. However, this higher level of viscosity smooths the shocks and eliminates other features of the flow. Hence, there arises a conflict between the requirements of accuracy and the need to reach a steady state rapidly.

II. Finite Volume Formulation

The Euler equations for an inviscid compressible flow can be written in divergence form as

$$\frac{\partial Q}{\partial t}+\frac{\partial f}{\partial x}+\frac{\partial g}{\partial y}+\frac{\partial h}{\partial z}=0 \tag{1}$$

where

$$Q=(\rho,\rho u,\rho v,\rho w,E)^t \tag{2a}$$

$$f=(\rho u,\rho u^2+p,\rho uv,\rho uw,(E+p)u)^t \tag{2b}$$

$$g=(\rho v,\rho uv,\rho v^2+p,\rho vw,(E+p)v)^t \tag{2c}$$

$$h=(\rho w,\rho uw,\rho vw,\rho w^2+p,(E+p)w)^t \tag{2d}$$

and for an ideal gas

$$p=(\gamma-1)[E-\rho(u^2+v^2+w^2)/2]. \tag{2e}$$

We can also write (1) in the form

$$\frac{\partial Q}{\partial t}+div(F)=0. \tag{1b}$$

We integrate (1) over a three dimensional cell and consider $Q_{i,j,k}$ as an approximation to the average of Q over the cell. Hence,

$$\frac{\partial Q_{i,j,k}}{\partial t}+\frac{\int\int\int divF\,dV}{\int\int\int dV}=0$$

or using the divergence theorem,

$$\frac{\partial}{\partial t}(VQ)_{ijk}+\int\int \vec{F}\cdot n\,dS=0. \tag{3}$$

Hence, the time change of the average Q is governed by the fluxes entering and leaving the cell [4,5].

One can arrive at a similar scheme by introducing new coordinates

$$\begin{aligned}\xi&=\xi(x,y,z)\\ \eta&=\eta(x,y,z)\\ \varsigma&=\varsigma(x,y,z)\end{aligned} \tag{4a}$$

such that ξ, η, ς = constant represent coordinate surfaces. Using this mapping technique together with finite differences leads to a formula similar to (3). However, now the volume is replaced by a Jacobian,

$$J=\frac{\partial(x,y,z)}{\partial(\xi,\eta,\varsigma)}. \tag{4b}$$

For an infinitesimally small cell the volume is equal to the Jacobian. Also, in two space dimensions the area of a quadrilateral is exactly equal to a central difference formula for the Jacobian i.e., if

$$\begin{aligned}J_{i+\frac{1}{2},j+\frac{1}{2}}=&(\xi_{i+1,j+1}-\xi_{i,j+1}+\xi_{i+1,j}-\xi_{ij})\cdot(\eta_{i+1,j+1}\\ &-\eta_{i+1,j}+\eta_{i,j+1}-\eta_{ij})/4-(\xi_{i+1,j+1}-\xi_{i+1,j}+\xi_{i,j+1}\\ &-\xi_{ij})\cdot(\eta_{i+1,j+1}-\eta_{i,j+1}+\eta_{i+1,j}-\eta_{ij})/4.\end{aligned} \tag{5}$$

J_{ij} gives the exact area of the quadrilateral with corners $(\xi_{i,j},\eta_{i,j})$, $(\xi_{i+1,j},\eta_{i+1,j})$, $(\xi_{i,j+1},\eta_{i,j+1})$, and $(\xi_{i+1,j+1},\eta_{i+1,j+1})$. However, in three dimensions there are differences between the finite volume formulation (3) and the finite difference formulation based on (4). In three dimensions one cannot find the volume of a three dimensional quadrilateral. If we assume that each face lies in a plane then we can divide the three dimensional cell into six pyramids and so calculate the volume. If the faces do not lie in a plane

then this gives an approximation to the volume. This approximation is no longer the same as that given by central differences of the Jacobian. Similar differences occur in the flux terms where normals to surfaces are required. The formula that comes from a finite volume approach is no longer exactly the same as that of a finite difference plus mapping approach. However, both formulas agree to second order accuracy. In a Cartesian mesh the finite volume and cell-centered finite difference approaches are the same.

III. Artificial Viscosity

Both the finite volume and the finite difference approaches lead to a pure central difference method for Cartesian grids. Though this scheme is stable for constant coefficient hyperbolic equations it is subject to instabilities that will prevent the convergence to a steady state. To force this convergence a fourth difference viscosity is added to the scheme. The fourth difference causes oscillations in the neighborhood of shocks. Hence, a nonlinear second difference is added to control oscillations near the shocks and the fourth difference is turned off. The total artificial viscosity, $\overline{V}$, is the sum of such second and fourth differences in each coordinate direction.

$$\begin{aligned}\overline{V}_{tot} &= \overline{V}^{\xi}_{i+\frac{1}{2},j,k} - \overline{V}^{\xi}_{i-\frac{1}{2},j,k} + \overline{V}^{\eta}_{i,j+\frac{1}{2},k} - \overline{V}^{\eta}_{i,j-\frac{1}{2},k} \\ &\quad + \overline{V}^{\xi}_{i,j,k+\frac{1}{2}} - \overline{V}^{\xi}_{i,j,k-\frac{1}{2}}\end{aligned} \tag{6}$$

Hence it is sufficient to describe these terms in the ξ direction. Since we only take differences at neighboring points the artificial viscosity is always in conservation form.

The first difference is defined as

$$D_{i+\frac{1}{2},j,k} = Q_{i+1,j,k} - Q_{i,j,k} \tag{7a}$$

and the second ξ difference is defined as

$$E_{i,j,k} = D_{i+\frac{1}{2},j,k} - D_{i-\frac{1}{2},j,k}. \tag{7b}$$

We then form the second and fourth differences. In particular the fourth difference is formed as a second difference of a second difference with positive weights [3,8]. Hence,

$$\overline{V}^{\xi}_{i+\frac{1}{2},j,k} = \epsilon^{(2)}_{i+\frac{1}{2},j,k} D_{i+\frac{1}{2},j,k} - (\epsilon^{(4)}_{i+1,j,k} E_{i+1,j,k} - \epsilon^{(4)}_{i,j,k} E_{i,j,k}). \tag{8}$$

Let,

$$\nu_{i,j,k} = \left| \frac{P_{i+1,j,k} - 2P_{i,j,k} + P_{i-1,j,k}}{P_{i+1,j,k} + 2P_{i,j,k} + P_{i-1,j,k}} \right|. \tag{9a}$$

Then $\nu_{i,j,k}$ is used to detect the location of shocks. When $\nu_{i,j,k}$ is large then the fourth difference is reduced. Other ways of normalizing the second difference of the pressure are also possible. Let,

$$\sigma_{i+\frac{1}{2},j,k} = K^{(2)} \max(\nu_{i-1,j,k}, \nu_{i,j,k}, \nu_{i+1,j,k}, \nu_{i+2,j,k}). \tag{9b}$$

We also multiply σ by a function of the Mach number to reduce σ near the surface. Finally let λ be a measure of the fluxes (this will be discussed in more detail). Then

$$\epsilon^{(2)}_{i+\frac{1}{2},j,k} = \lambda_{i+\frac{1}{2},j,k} \sigma_{i+\frac{1}{2},j,k} \tag{9c}$$

$$\epsilon^{(4)}_{i,j,k} = \lambda_{i,j,k} \max(0, K^{(4)} - \sigma_{i,j,k}). \tag{9d}$$

Let, $A = \frac{\partial \overline{F}}{\partial Q}, B = \frac{\partial \overline{G}}{\partial Q}, C = \frac{\partial \overline{H}}{\partial Q}$, where $\overline{F}, \overline{G}, \overline{H}$ are the fluxes in the coordinate system (ξ, η, ς). The original code chose λ as

$$\lambda^{\xi} = \lambda^{\eta} = \lambda^{\varsigma} = \rho(A) + \rho(B) + \rho(C) \tag{10a}$$

where ρ is the the spectral radius of the matrix. For problems with a highly stretched mesh it was found [1,3,8,11,12] that for increased accuracy one should choose

$$\lambda^{\xi} = \rho(A),\ \lambda^{\eta} = \rho(B),\ \lambda^{\xi} = \rho(C). \tag{10b}$$

$\kappa^{(2)}$, $\kappa^{(4)}$ are constants that determine the level of the second and fourth differences. These constants are given as input to the code. In the result section these will be varied to see their effect both on the accuracy of the solution and on their convergence rate.

In all our calculations we use a C grid in each plane. It was found important to calculate the artificial viscosity across the wake and not to treat the wake as a solid surface. In the spanwise direction we use either an H or an O grid. The H grid leads to a simpler topology but does not give sufficient resolution near the wing tip. With the O mesh care must be taken to reflect the proper points across the wake and near the wing tip. This is especially important for the fourth difference in the ξ direction which requires several points on the other side of the wake.

IV. Results

We first consider flow past an isolated ONERA M6 wing with $M_\infty = 0.84$ and $\alpha = 3.06^0$. We use a coarse $96 \times 16 \times 16$ C-H mesh. In Figure 1a, 1b we show the C_p plots over the upper surface. For this case

$$\begin{aligned}\kappa^{(2)} &= 2./2. \\ \kappa^{(4)} &= 2./64.\end{aligned} \tag{11a}$$

In Figure 1c we plot the convergence history for this case. A five stage Runge-Kutta scheme was used with two evaluations of the artificial viscosity. This scheme was used once per iteration on the finest grid, twice on the next finest grid and three times on all coarser grids. On the way up from coarser to finer grids no smoothing was used and the changes were just interpolated to the next finer grid. With this scheme we were able to reduce the mean density residual by 9 orders of magnitude after 100 iterations on the finest mesh. Using a FMG method the initial condition was obtained by using 10 iterations each on two coarser grids. These convergence rates are close to those obtained by Jameson [6] using a nodal scheme. Hence, we see that there are no major differences in convergence rates and robustness between the cell-centered and the nodal versions of the multi-stage methods.

In Figure 2 we plot the same case but with

$$\begin{aligned}\kappa^{(2)} &= 0.5/2. \\ \kappa^{(4)} &= 0.5/64.\end{aligned} \tag{11b}$$

We see that now the shocks are much sharper and that other features of the flow are more pronounced. In addition, the total lift was lowered from .299 to .287 and the drag was changed from .0174 to 0.147. With this reduced $\kappa^{(2)}$, $\kappa^{(4)}$ the lift and drag are close to that given in the finer mesh

of Figure 3. However, now the convergence rate is reduced to a 5 order reduction within the 100 iterations.

In Figure 3 we plot the same physical case but using a finer $192 \times 32 \times 32$ C-O mesh. Looking carefully at individual stations one can again see that the lower viscosity level leads to sharper profiles but at the expense of a slightly reduced convergence rate. With this finer mesh there is much less of a sensitivity to the constants in the artificial viscosity compared with the coarse mesh (see also [12]).

In Figure 4 we plot the convergence rate for a supersonic flow about a delta wing. For this case a $128 \times 24 \times 16$ C-H mesh was used supplied by Moitra [7]. This further demonstrates the robustness of the present code over different configurations and different flight conditions.

References

[1] Caughey, D. A., A Diagonal Implicit Algorithm for Compressible Flow Calculations, Adv. Computer Methods PDE's VI, pp. 270-277, R. Vichnevetsky, R. S. Stepleman (editors), IMACS, 1987.

[2] Caughey, D. A., Turkel, E., Effects of Numerical Dissipation on Finite-Volume Solutions of Compressible Flow Problems, AIAA-88-0621.

[3] Chima, R. V., Turkel, E., Schaffer, S., Comparison of Three Explicit Multigrid Methods for the Euler and Navier-Stokes Equations, AIAA-87-0602.

[4] Jameson, A., Schmidt, W., Turkel, E., Numerical Solutions of the Euler Equations by Finite Volume Methods using Runge-Kutta Time-Stepping Schemes, AIAA-81-1259.

[5] Jameson, A., Baker, T. J., Multigrid Solutions of the Euler Equations for Aircraft Configurations, AIAA-84-0093.

[6] Jameson, A., A Vertex Based Multigrid Algortihm for Three Dimensional Compressible Flow Calculations, American Society Mech. Eng., AMD - Vol. 78, T. E. Tezcuyar, T. J. R. Hughes (ed.), pp. 45-73, 1986.

[7] Moitra, A., Numerical Solution of the Euler Equations for High-speed Blended Wing-Body Configurations, AIAA-85-0123.

[8] Swanson, R. C., Turkel, E., Artificial Dissipation and Central Difference Schemes for the Euler and Navier-Stokes Equations, AIAA 8th CFD Conference, AIAA-87-1107-CP.

[9] Turkel, E., Acceleration to a Steady State for the Euler Equations, Numerical Methods for the Euler equations of Fluid Dynamics, pp. 281-311, F. Angrand, et al. (editors), SIAM, 1985.

[10] Turkel, E., Accuracy of Schemes with Nonuniform Meshes for Compressible Fluid Flows, Applied Numer. Math., Vol. 2, pp. 529-550, 1986.

[11] Vatsa, V. N., Accurate Numerical Solutions for Transonic Viscous Flow Over Finite Wings, J. Aircraft, Vol. 24, pp. 377-385, 1987.

[12] Vatsa, V. N., Thomas, J. J., Wedan, B. W., Navier-Stokes Computations of Prolate Spheroids at Angle of Attack, AIAA-87-2627-CP.

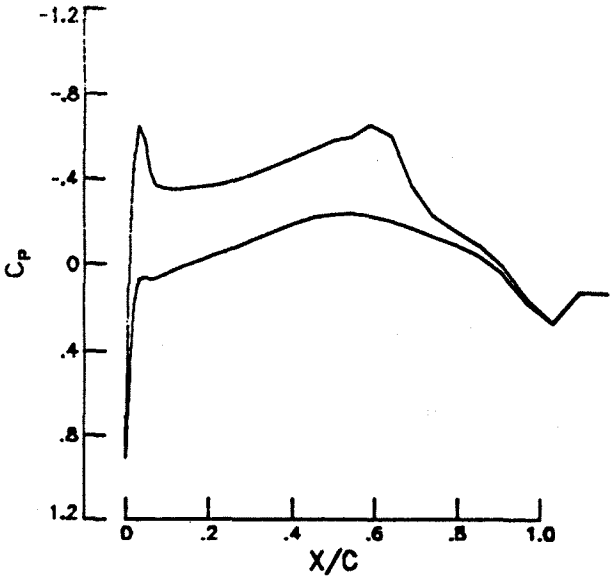

Figure 1a. ONERA M6 wing, $M_\infty = .84$, $\alpha = 3.06$, $96 \times 16 \times 16$ C-H mesh, $\kappa^{(2)} = \frac{1}{4}$, $\kappa^{(4)} = \frac{1}{128}$, station = 0.05.

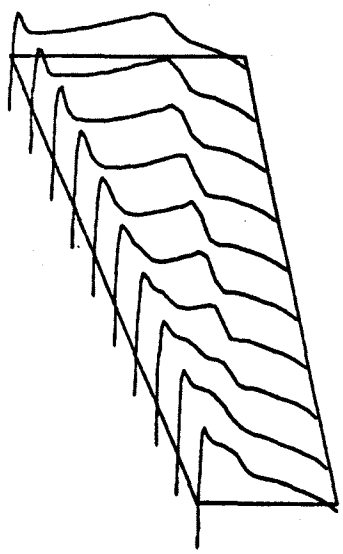

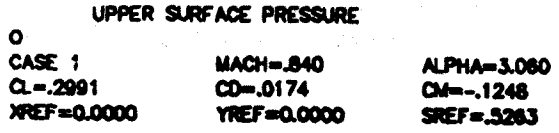

Figure 1b. Upper surface pressure plot.

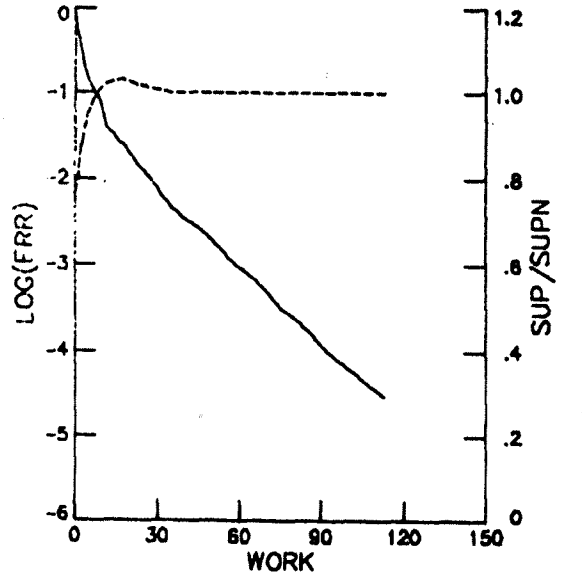

O
CASE 1 NMESH=3 NCYC=100
RES1=.602 x 10^0 RESN=.175 x 10^{-4} RATE=.9117
SUP1=675 SUPN=884 WORK=112.92

Figure 1c. Convergence plot of average ρ residual.

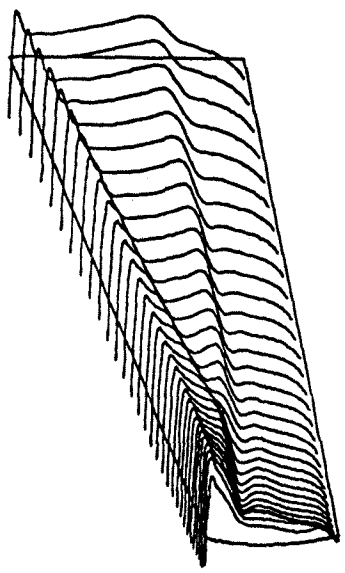

UPPER SURFACE PRESSURE
O
CASE 1 MACH=.840 ALPHA=3.060
CL=.2870 CD=.0142 CM=-.1153
XREF=0.0000 YREF=0.0000 SREF=.5308

Figure 2b. Upper surface pressure.

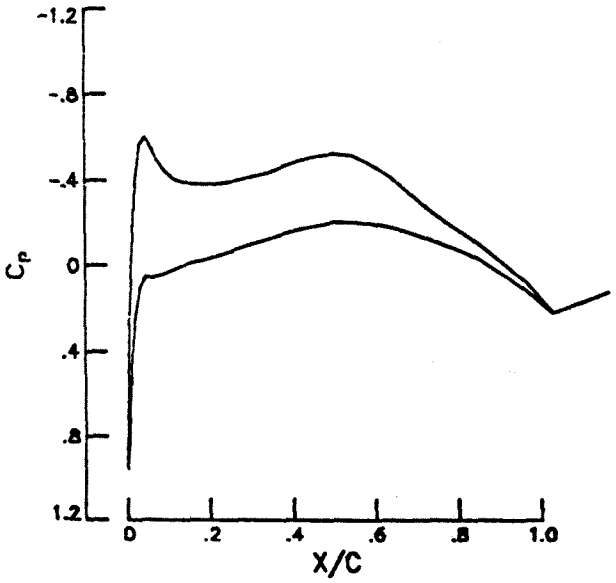

Figure 2a. Same as Figure 1a with $\kappa^{(2)} = 1$, $\kappa^{(4)} = \frac{1}{32}$.

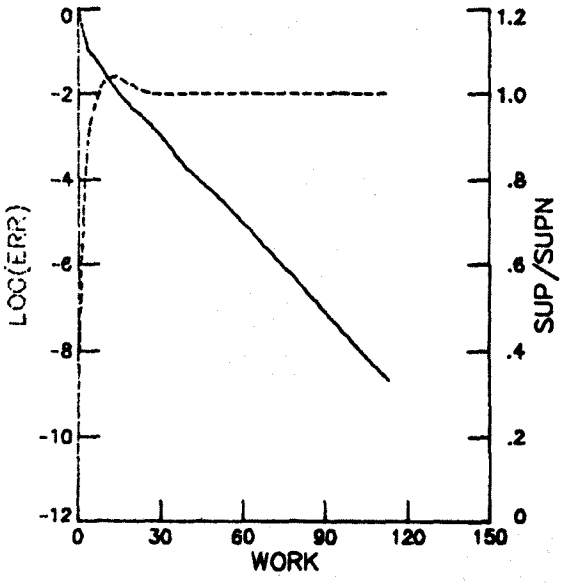

O
CASE 1 NMESH=3 NCYC=100
RES1=.602 x 10^0 RESN=.123 x 10^{-6} RATE=.8376
SUP1=280 SUPN=779 WORK=112.92

Figure 2c. Convergence history.

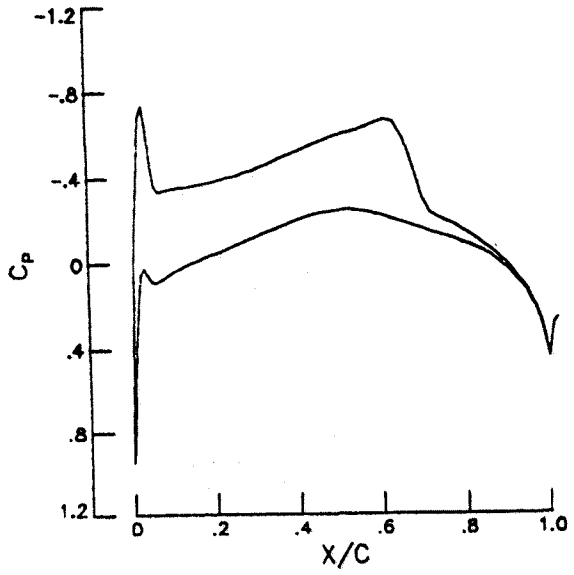

Figure 3a. Same as Figure 1 with $192 \times 32 \times 32$ C-0 mesh. $\kappa^{(2)} = \frac{1}{2}, \kappa^{(4)} = \frac{1}{64}$.

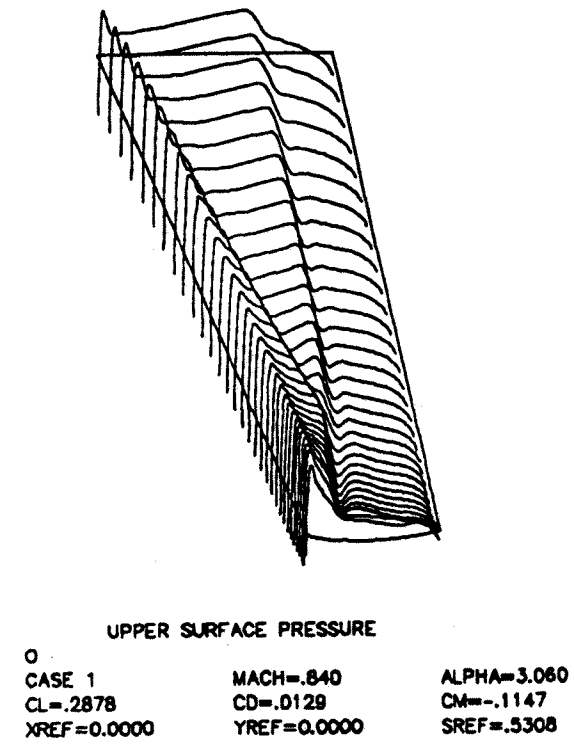

Figure 3b. Upper surface pressure.

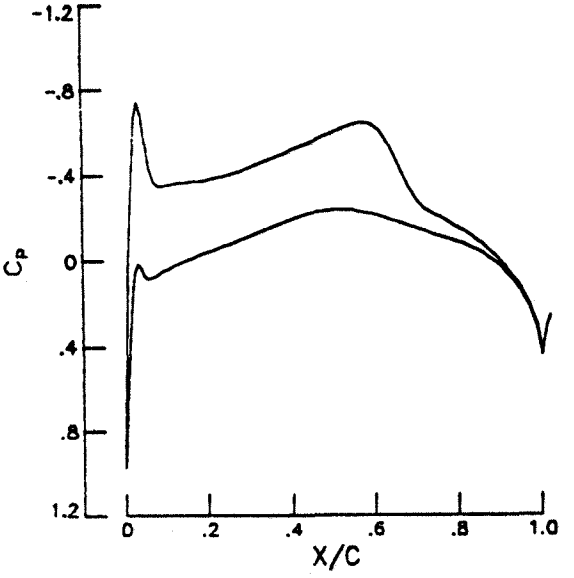

Figure 3c. Same as Figure 3a with $\kappa^{(2)} = 1$, $\kappa^{(4)} = \frac{1}{32}$.

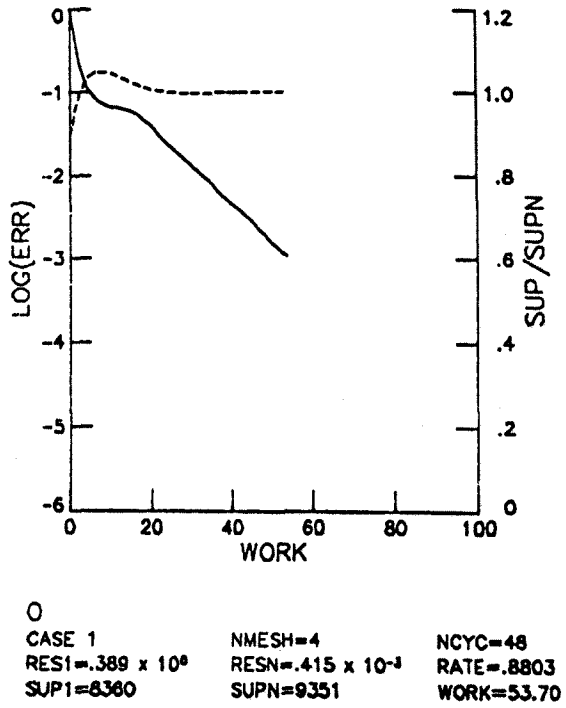

Figure 3d. Convergence history for Figure 3c. Note: Scale is different than Figure 1c and 2c since fewer iterations were done.

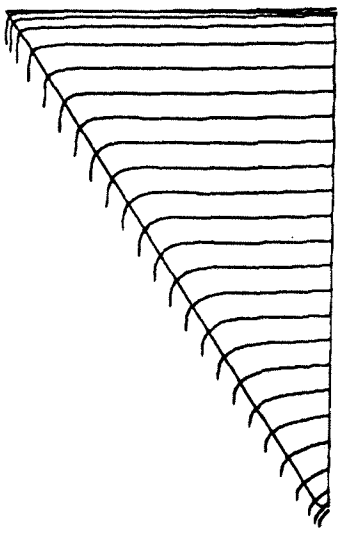

UPPER SURFACE PRESSURE

M

CASE 1	MACH=2.500	ALPHA=1.200
CL=.0156	CD=.0090	CM=-.0180
XREF=0.0000	YREF=0.0000	SREF=.9552

Figure 4a. Delta wing $M_\infty = 2.5,\ \alpha = 1.2°$.

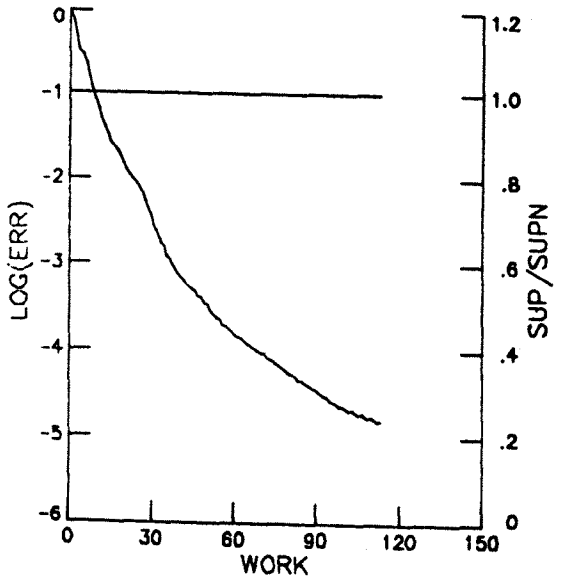

M

CASE 1	NMESH=3	NCYC=100
RES1=.168 x 10^{-1}	RESN=.263 x 10^{-6}	RATE=.9067
SUP1=73728	SUPN=73728	WORK=112.92

Figure 4b. Convergence history.